DOI: 10.1002/ejic.201100676

Can Hydrophobic Interactions Influence Supramolecular Aggregation in Self-Assembled Organic–Inorganic Hybrid Structures?

Kirsten Heussner,[a] Mathias Grabau,[a] Johannes Forster,[a] and Carsten Streb*[a]

Keywords: Supramolecular chemistry / Aggregation / Crystal engineering / Polyoxometalates / Organic-inorganic hybrid composites / Amphiphiles / Hirshfeld analysis

This study aims to provide insights into the ability of amphiphilic cations to influence the assembly of hybrid organic-inorganic crystal lattices using hydrophobic interactions. To investigate the hypothesis, a prototype amphiphilic cation, *tert*-butyldiethanolammonium, was employed together with molybdenum oxide clusters of increasing size and charge in the self-assembly of type I hybrid systems. The molybdate clusters were used as model inorganic building blocks as they can be formed in situ and their size and charge can be adjusted by pH control. Using this strategy, three hybrid structures were obtained and characterized using single-crystal X-ray diffraction, theoretical bond valence sum calculations, elemental analysis, FTIR spectroscopy, thermogravimetry and theoretical Hirshfeld analysis. Heptamolybdate $Na_5[t\text{BuNH}(C_2H_4OH)_2][Mo_7O_{24}]\cdot ca.\,14H_2O$ (**1**) was isolated, which features sodium-linked dimeric cluster species. In addition, octamolybdate $[t\text{BuNH}(C_2H_4OH)_2]_4[Mo_8O_{26}]\cdot ca.\,4H_2O$ (**2**) was isolated, which incorporates a complex cationic sodium network that contains isolated octadecanuclear sodium clusters. At low pH levels (below pH 2), $[t\text{BuNH}(C_2H_4OH)_2]_{14}[Mo_{36}O_{112}(H_2O)_{16}][Mo_{36}O_{112}(H_2O)_{14}\{t\text{BuNH}(C_2H_4OH)_2\}_2]\cdot ca.\,36H_2O$ (**3**) was obtained, which is based on a 36-centre molybdenum oxide cluster. Crystallographic analysis of the assemblies showed that the formation of hydrophobic regions within the crystal lattice is affected by the size of the inorganic building blocks employed. In **1** and **2**, the hydrophobic *tert*-butyl groups of the amphiphilic cations aggregate into hydrophobic assemblies. In contrast, the structural arrangement in **3** is dominated by the large inorganic cluster and the organic cations are incorporated as isolated units. This behaviour is further supported by theoretical Hirshfeld surface analysis of the organic counterions, which suggests that, with increasing cluster size, the contribution of long-range, hydrophobic intermolecular interactions decreases, which is in line with the crystallographic analysis for **1**–**3**.

Introduction

The controlled assembly of supramolecular architectures based on molecular precursors holds great promise for the design of functional materials with wide ranging applications.[1] One key feature required for these assemblies is the ability to engineer compartmentalized crystal lattices, which would allow the formation of regions with different chemical and physical properties.[2] Such systems are highly desirable for a large variety of applications from selective molecular sorption[3] and the design of hydrogen storage sites[4] to the creation of nanostructured materials with sophisticated architectures and new properties.[5] One route to the formation of these systems could be the self-assembly of amphiphilic organic cations with anionic inorganic building blocks that range from Zintl anions,[6] carboranes[7] and fullerides[8] to metal sulfide[9] and metal oxide clusters,[10] which result in the formation of class I[11] hybrid organic-inorganic systems.[12,13]

In this initial study, the electrostatically-controlled formation of organic-inorganic hybrid systems was investigated with a range of experimental and theoretical analyses. The aim was to identify ways of directing the self-assembly so as to guide the resulting architecture into separate hydrophilic and hydrophobic regions.[14] Here, molecular molybdenum oxide clusters, so-called polyoxomolybdates, were used as a representative model system for anionic, inorganic building units.[13,15] The molybdenum oxide cluster system is ideally suited as it allows the targeting of a range of cluster structures under comparable reaction conditions by controlled variation of the solution pH.[16] In addition, a prototype amphiphilic organic counterion, *tert*-butyldiethanolammonium (BDA), was introduced, which is known to establish hydrophobic interactions through the *tert*-butyl side chain as well as coordinative and hydrogen-bonding interactions through the hydroxyethyl groups. In addition, non-directed electrostatic Coulomb interactions can be formed between the positively charged ammonium group and neighbouring cluster anions.[17] In particular the presence of the bulky *tert*-butyl substituent was hypothesized to al-

[a] Department Chemistry and Pharmacy, Institute of Inorganic Chemistry II, Friedrich-Alexander-University Erlangen-Nuremberg,
Egerlandstr. 1, 91058 Erlangen, Germany
Fax: +49-9131-27367
E-mail: carsten.streb@chemie.uni-erlangen.de
www.strebgroup.net

Supporting information for this article is available on the WWW under http://dx.doi.org/10.1002/ejic.201100676.

low the formation of hydrophobic regions within the crystal lattice, owing to its rigid and sterically demanding nature (Scheme 1).

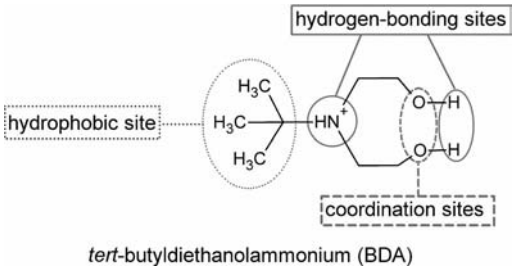

Scheme 1. Potential intermolecular interaction sites of the BDA cation.

When discussing hydrophobic interactions in a supramolecular system or crystal lattice it should be noted that the so-called hydrophobic effect is observed when nonpolar molecules or molecular regions (the *tert*-butyl substituent of the BDA cation here) are introduced in a polar solvent such as water. In the case of water, the vast hydrogen-bond network is interrupted by the presence of a nonpolar moiety, which results in the formation of a hydrogen-bonded solvation "cage" of water molecules around the nonpolar moiety. As a consequence, the translational and rotational entropy of the water molecules is reduced, which results in an increase in the Gibbs free energy. In order to minimize this energetically unfavourable effect, hydrophobic molecules often aggregate into hydrophobic pockets to minimize the surface area exposed to the bulk solvent.[18] This behaviour is most pronounced in large molecular systems such as proteins where a multitude of hydrophobic amino acid residues contribute to tertiary folding through the formation of a hydrophobic internal protein core. For the system under investigation, one of the main questions was whether the comparatively small hydrophobic *tert*-butyl groups would allow the observation of hydrophobic interactions (Scheme 1).

Results and Discussion

{Mo_7}-Based Hybrid Architecture

$Na_5[t\text{BuNH}(C_2H_4OH)_2][Mo_7O_{24}]\cdot$ca. $14H_2O$ (**1**) was obtained from the reaction of an aqueous solution of Na_2MoO_4 with *tert*-butyldiethanolamine. The solution pH was adjusted to 5.5 with aqueous HCl (1 M), which allowed the in situ formation of the heptanuclear $[Mo_7O_{24}]^{6-}$ inorganic building block by controlling the molybdate speciation in solution.[19] The main inorganic building unit of **1** is the well-known heptanuclear isopolyoxomolybdate cluster $[Mo_7O_{24}]^{6-}$ ({Mo_7}). {Mo_7} can be described as a six-membered ring formed from six octahedrally coordinated Mo^{VI} centres in a boat conformation with the seventh Mo^{VI} centre located in an apical position. Bond valence sum (BVS) calculations[20] indicate that all the Mo centres are fully oxidized d^0 centres and that none of the oxo ligands are protonated.

In the lattice of **1**, the {Mo_7} cluster units self-assemble into dimeric, dumbbell-shaped, sodium-linked {Mo_7}–Na–{Mo_7} units ([Na{Mo_7}$_2$]). Each {Mo_7} cluster features a set of three terminal oxo ligands arranged in a triangular fashion, which form an ideal *fac* binding site for octahedral metal centres. It is this binding site that is occupied by the linking sodium cation to form three Na–O coordination bonds to each {Mo_7} cluster, thereby linking two neighbouring {Mo_7} units, with Na–O distances of d_{Na-O} = 2.4–2.6 Å. The resulting [Na{Mo_7}$_2$] aggregate features dimensions of approximately 1.95 nm along the main molecular axis and shows idealized C_{2h} symmetry. In **1**, the [Na{Mo_7}$_2$] dimers are arranged in a coparallel fashion with the main dimer axis oriented along the crystallographic [1 1 0] direction (Figure 1). Along the crystallographic *c* axis, the dimers are arranged in an ABAB-type layered fashion with Na···Na distances of ca. 1.1 nm between the neighbouring dimers.

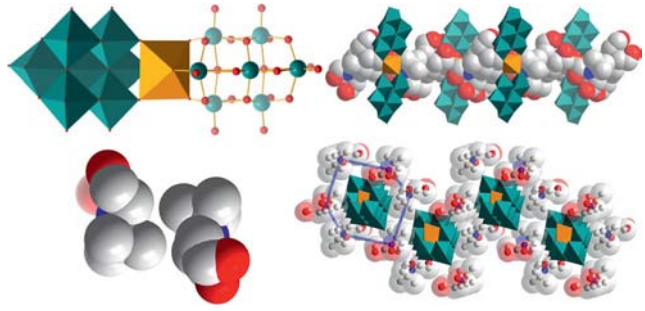

Figure 1. Left: Representation of the [Na{Mo_7}$_2$] dimer in **1**, which shows the sodium-linked $[Mo_7O_{24}]^{6-}$ isopolyoxomolybdate clusters (top) and space-filling representation of the hydrophobic aggregates formed by the BDA cations (bottom). Right: Arrangement of the [Na{Mo_7}$_2$] dimers in the crystal lattice of **1**. The colinear arrangement (top) and the ABAB-zigzag propagation (bottom) are shown. The encapsulating organic counterions are highlighted in the space-filling representation and their hexagonal arrangement around the [Na{Mo_7}$_2$] dimers is highlighted by a blue hexagon. Colour scheme Mo: green, O: red, Na: orange, [MoO_6] polyhedra: green, [NaO_6] polyhedra: orange. Interlayer sodium counterions and H atoms are omitted for clarity.

Within the ABAB layers, stabilization and separation of the [Na{Mo_7}$_2$] dimers is achieved by the BDA counterions, which form hydrophobic regions between pairs of neighbouring BDA cations to create close contacts (minimum d_{C-C} = 3.72 Å) between the hydrophobic, bulky *tert*-butyl substituents. This unusual packing feature results in the effective isolation of the [Na{Mo_7}$_2$] dimers in the crystal lattice so that each dimer is encapsulated by six BDA counterions in a hexagonal fashion (Figure 1). The hexagonal packing of the BDA cations around the [Na{Mo_7}$_2$] dimers results in the high-density intralayer packing of the organic counterions in **1**. In contrast, the interlayer spaces between adjacent layers of [Na{Mo_7}$_2$] dimers are occupied exclusively by sodium cations, which act as counterions and add structural stability to the network by coordination to

{Mo_7}-based oxo ligands. Detailed analysis shows that these sodium cations are not randomly distributed and do not form infinite aggregates; instead, octadecanuclear, isolated {Na_{18}} clusters are formed, which are embedded between sets of {Mo_7} clusters, and can be considered as stabilized molecular assemblies (Figure 2).

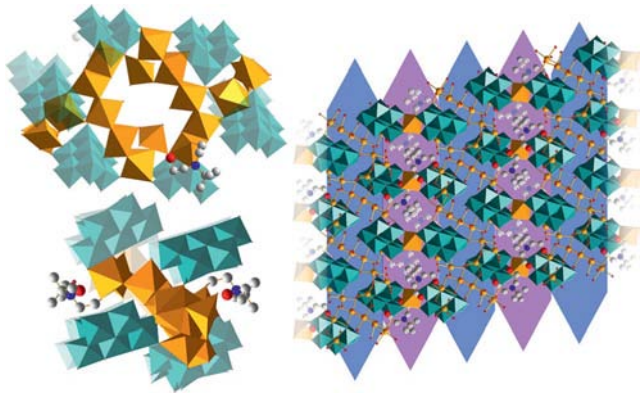

Figure 2. Left: Illustration of the isolated {Na_{18}} cluster embedded between {Mo_7} units in **1**, which highlights its butterfly shape (top) and showing the encapsulation by {Mo_7} clusters and BDA counterions (bottom). Right: Rationalization of the full crystal packing showing alternating layers of BDA-stabilized [Na{Mo_7}$_2$] dimers (highlighted by purple arrows) and sets of {Na_{18}} aggregates in the interlayer regions between the dimers (highlighted by blue arrows). Colour scheme {Mo_7}: green polyhedra, [NaO_6]: orange polyhedra, C: grey spheres, N: blue spheres, O: red spheres. H atoms are omitted for clarity.

It is suggested that the {Na_{18}} clusters in **1** are a result of the crystal packing and are therefore only present in the solid state. Structurally, the {Na_{18}} units are based on a ring-shaped dodecanuclear assembly of 12 sodium ions, which are all coordinated by cluster-based oxo ligands and water molecules that stabilize this arrangement. In addition, three sodium centres are located on either side of the ring; these centres are additionally supported by the coordination of a BDA hydroxy group. The resulting motif resembles a butterfly and can be rationalized as {Na_{18}} = [{Na_{12}}$_1${Na_3}$_2$] (Figure 2). The observation of the extended {Na_{18}} clusters also suggests that further studies in the absence of inorganic cations (e.g. starting from MoO_3 as the molybdate source) might allow the incorporation of additional BDA counterions and result in the formation of larger hydrophobic domains.

{Mo_8}-Based Hybrid Architecture

In order to investigate the interactions of the amphiphilic, organic BDA cations with larger molybdate cluster systems, crystallizations were carried out in the same reaction system as described above, however, the pH was set to 4.0 to target the well-known octanuclear β-[Mo_8O_{26}]$^{4-}$ cluster.[21] This approach allowed the isolation and characterization of [*t*BuNH(C_2H_4OH)$_2$]$_4$[Mo_8O_{26}]·ca.$4H_2O$ (**2**). As expected, **2** contains the octanuclear β-[Mo_8O_{26}]$^{4-}$ isopolyoxomolybdate cluster[21] ({Mo_8}) as the main inorganic structural backbone. The {Mo_8} cluster consists of eight octahedrally coordinated Mo^{VI} centres, which are arranged in two planar [Mo_4O_{13}] building units that are centrally linked by four bridging oxo ligands.

In the crystal lattice of **2**, the {Mo_8} units form hybrid 1D chains, which propagate along the crystallographic [1 0 1] direction. Within these chains, the {Mo_8} units are linked by dimeric, hydrogen-bonded aggregates formed between two BDA cations. In these supramolecular {BDA}$_2$ dimers, the organic cations aggregate such that two internal O–H···N hydrogen bonds ($d_{O\cdots N}$ = 2.92 Å) are formed between one of the pendant hydroxyethyl arms of one BDA molecule and the central nitrogen atom of the second molecule and vice versa. In addition to these internal hydrogen-bonded interactions, the second hydroxyethyl arm of each BDA cation forms strong OH···O hydrogen bonds ($d_{O\cdots O}$ = 2.83 Å) to a μ_2-oxo ligand of the adjacent {Mo_8} cluster. As this interaction occurs on either side of the {BDA}$_2$ dimer, the molybdate clusters are linked into infinite hydrogen-bonded 1D chains where the repeating unit is [–BDA–{Mo_8}–BDA–]$_\infty$ with distances between neighbouring clusters of ca. 1.1 nm (Figure 3).

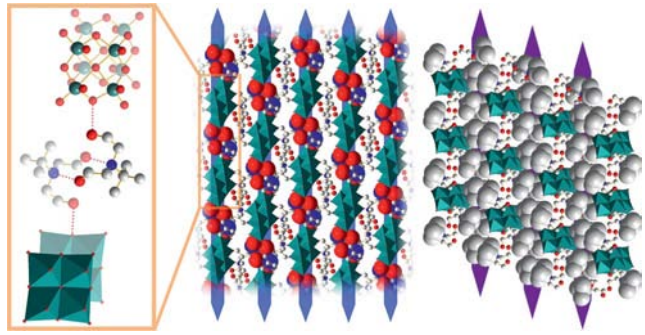

Figure 3. Left: Illustration of the repeating unit of the infinite hydrogen-bonded [–BDA–{Mo_8}–BDA–]$_\infty$ chain in **2**, which shows the {Mo_8} cluster in a ball-and-stick representation (top) and polyhedral representation (bottom). The O–H···N hydrogen bonds in the {BDA}$_2$ dimer are highlighted by dotted red lines. Centre: Representation of the infinite hydrogen-bonded 1D chains (highlighted by blue arrows), which propagate along the crystallographic [1 0 1] direction. Right: Illustration of the hydrophobic columnar structures (highlighted by purple arrows) formed by self-aggregation of the hydrophobic *tert*-butyl substituents (grey space-filling representation) of the BDA cations. Colour scheme Mo: green, O: red, C: grey, N: blue, {Mo_8}: green polyhedra.

In addition to this primary hydrogen-bonded assembly, a second assembly pattern can be observed. As already seen in **1**, the hydrophobic *tert*-butyl groups of the BDA cations in **2** self-assemble into hydrophobic compartments within the crystal lattice. However, in contrast to the isolated hydrophobic regions observed for the BDA dimers in **1**, the BDA cations in **2** assemble into 1D hydrophobic columnar structures along the crystallographic *a* axis (Figure 3). These columns are formed primarily by the *tert*-butyl substituents of the {BDA}$_2$ dimers that connect the molybdate clusters. However, two additional nondimeric BDA cations are located in the interchain regions between the infinite 1D {Mo_8} chains, which complete the hydrophobic columnar arrangement (Figure 3). The *tert*-butyl groups of these

BDA cations contribute to the formation of the hydrophobic channels, whereas their hydrophilic hydroxyethyl arms stabilize the lattice by forming strong hydrogen-bonded interactions with oxo ligands on the {Mo_8} clusters ($d_{O\cdots O}$ = 2.74 Å) and to lattice water molecules.

{Mo_{36}}-Based Hybrid Architecture

In order to understand whether these hydrophobic interactions are structurally relevant in very large molybdate cluster systems, we opted to investigate the BDA/molybdate systems at low pH values where larger clusters are typically formed. From such an experimental setup at pH = 2.0, we were able to isolate and characterize $[t\text{BuNH}(C_2H_4OH)_2]_{14}[Mo_{36}O_{112}(H_2O)_{16}][Mo_{36}O_{112}(H_2O)_{14}\{t\text{BuNH}(C_2H_4OH)_2\}_2]\cdot$ ca. $36H_2O$ (**3**). Structural analysis shows that the main inorganic building unit in **3** is a 36-centre molybdate cluster, $[Mo_{36}O_{112}(H_2O)_{16}]^{8-}$ ({Mo_{36}}), which is well-known to form in highly acidic molybdate solutions.[22] The cluster can be rationalized as a dimeric unit formed by the linkage of two bowl-shaped {Mo_{17}} subunits that are centrally linked by two mononuclear {Mo_1} connectors, which give the overall formula {Mo_{36}} = [{Mo_{17}}$_2${Mo_1}$_2$]. As a result of this assembly, the cluster features an overall ellipsoidal shape and dimensions of ca. 2.1 × 1.5 × 1.1 nm (Figure 4).

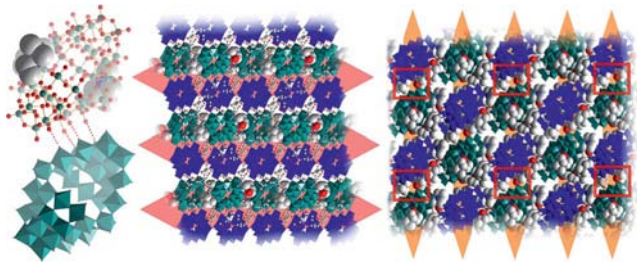

Figure 4. Left: Illustration of the hydrogen-bonded {Mo_{36}} clusters in **3**, which highlights the BDA-modified o-{Mo_{36}} cluster in ball-and-stick representation (top) and the purely inorganic i-{Mo_{36}} unit in polyhedral representation (bottom). The close hydrogen-bonded contacts are emphasized with red dotted lines. Centre: Illustration of the crystal packing in **3**, which shows the linear, staggered arrangement of the two cluster types along the crystallographic *b* axis (o-{Mo_{36}}: green polyhedra; i-{Mo_{36}}: blue polyhedra). Right: Illustration of the encapsulation of the cluster units by the bulky organic BDA counterions. The hydrogen-bonded chains of o-{Mo_{36}}- and i-{Mo_{36}}, which propagate along the crystallographic [1 1 0] direction, are highlighted by orange arrows. The areas where intercluster hydrogen bonds dominate the crystal packing are highlighted by red rectangles. Colour scheme Mo: green spheres/polyhedra, O: red spheres, C: grey spheres, N: blue spheres. Hydrogen atoms and water of crystallization are omitted for clarity.

The asymmetric unit of **3** contains two crystallographically independent {Mo_{36}} clusters; the first {Mo_{36}} unit (i-{Mo_{36}}; i: inorganic) is a purely inorganic metal oxide unit where the molybdenum centres are exclusively coordinated by 112 oxo and 16 water ligands, which gives the overall formula i-{Mo_{36}} = $[Mo_{36}O_{112}(H_2O)_{16}]^{8-}$. The positions of the sixteen water molecules were identified by structural analysis and theoretical BVS calculations. It was shown that the water ligands are distributed symmetrically over the cluster shell and can be separated into four μ_2-bridging water molecules ($d_{Mo-\mu_2\text{-}OH_2}$ = 2.4–2.5 Å) and twelve terminal water ligands with typical bond lengths of 2.3–2.4 Å. The molybdate framework of the second {Mo_{36}} cluster (o-{Mo_{36}}; o: organic) in **3** is isostructural to the cluster shell of the i-{Mo_{36}} unit; however, the o-{Mo_{36}} unit is organically modified by two coordinated BDA cations located on peripheral binding sites that are occupied by water ligands in the i-{Mo_{36}} unit. The BDA cations bind to the cluster by coordination of one hydroxyethyl oxygen atom to a Mo^{VI} centre on the cluster periphery to give the formula $[Mo_{36}O_{112}(H_2O)_{14}\{t\text{BuNH}(C_2H_4OH)_2\}_2]^{6-}$. The two BDA cations are located on opposite sides of the cluster, which increases the diameter of the cluster shell from 1.5 to 1.8 nm (Figure 4).

In the crystal lattice of **3**, the two {Mo_{36}} units are arranged as infinite 1D hydrogen-bonded chains formed by an alternating arrangement of i-{Mo_{36}} and o-{Mo_{36}} clusters (minimum distance between clusters: 3.15 Å) linked by sets of hydrogen bonded water ligands and BDA cations (Figure 4). Within the chains, the clusters are arranged in a side-on fashion; however, along the chain propagation direction, the clusters are not arranged in a coparallel fashion but feature a torsion angle of ca. 17° between the main molecular planes. Within the planes, the organic BDA cations coordinated to either side of the {Mo_{36}} clusters protrude above and below the 1D chain and act as spacers between neighbouring chain sections to prevent any close interchain interactions.

The 1D hydrogen-bonded chains in **3** are further stabilized within the lattice by 14 BDA cations and ca. 34 water molecules that form an extensive hydrogen-bonded network, which stabilizes the chains themselves (intrachain hydrogen bonds) and forms extensive interchain hydrogen bonds (Figure 4). From the crystal packing it is evident that the effects of the hydrophobic interactions observed in **1** and **2** are much less pronounced in **3**. From the detailed structural analysis it can be suggested that this behaviour is due to the increased size of the {Mo_{36}} units in **3** compared with the {Mo_7} and {Mo_8} units in **1** and **2**, respectively. Although the molybdate clusters in **1** and **2** are comparable in size to the BDA cations, the {Mo_{36}} unit in **3** is much larger and hence the steric constraints imposed by the packing requirements of this cluster do not allow any pronounced packing effects based on comparatively weak hydrophobic interactions between the *tert*-butyl substituents on the BDA cations. As a result, the BDA units simply aggregate in the voids formed between adjacent clusters to minimize the steric strain within the crystal lattice.

Additional experiments were conducted on **1**–**3** to investigate whether they are only formed at the given molybdate:BDA molar ratios or whether they represent a crystal phase that is obtained over a wider range of molar ratios. Initial observations suggest that **1**–**3** are indeed not only formed at the ratio reported but also form when one reactant is increased or decreased by up to 10 mol-%. Further changes to the reaction ratio often resulted in the formation of precipitates or systems that did not produce any solid

products. None of the reactions performed yielded crystalline products other than **1**–**3**, which suggests that these are the preferred phases in the reaction range under investigation.

Theoretical Hirshfeld Analysis of the BDA Cations in 1–3

In order to evaluate the intermolecular interactions around the BDA cations in **1**–**3**, a theoretical Hirshfeld analysis based on their crystal structures was conducted.[23] In short, the Hirshfeld method allows the facile analysis of intermolecular contacts within a crystal lattice. Using a computational algorithm based on spherically averaged Hartree–Fock electron density functionals,[24] isosurfaces for molecular fragments within a crystal lattice are calculated. These isosurfaces can be interpreted as boundaries between separated molecular structures. The resulting Hirshfeld surface indicates intermolecular distances using a colour-coded scheme and gives an immediate representation of the molecular regions where short and long intermolecular distances (i.e. strong and weak intermolecular interactions) are observed. The advantage of this approach is that both strong *and* weak intermolecular interactions are instantly recognized, whereas in traditional crystallographic search algorithms (i.e. those based on intermolecular distances smaller than the sum of the van der Waals radii) tend to highlight strong intermolecular interactions (e.g. hydrogen bonds) only. Due to the focus of this investigation and owing to the structural complexity of **1**–**3**, the Hirshfeld analysis focussed particularly on the intermolecular interactions of the BDA cations with particular emphasis on the interactions observed around their hydrophobic *tert*-butyl groups.

When comparing the hydrophobic *tert*-butyl groups of the BDA counterions in **1**–**3**, a general trend can be seen.

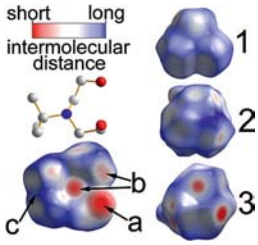

Figure 5. Hirshfeld analysis of representative BDA cations in **1**–**3**. Left: General Hirshfeld analysis of a BDA cation, which highlights a range of intermolecular interactions: (a) strong C–O···Na coordinative interaction (short intermolecular contact); (b) O–H···O and N–H···O hydrogen bonds; (c) hydrophobic van der Waals interactions between adjacent *tert*-butyl substituents (long intermolecular interactions). Right: Illustration of the Hirshfeld surfaces of representative BDA cations in **1**–**3**. The BDA cations in **1** and **2** show mainly long-range interactions, which suggest hydrophobic interactions only (few shorter contacts are observed in **2**). In **3**, several short C–H···O interactions are observed between the BDA cation and the cluster anion, indicating that the amount of hydrophobic stabilization is reduced and the *tert*-butyl groups are in closer contact with the cluster shell. For full analysis see Figure S4, Supporting Information.

In **1**, only long intermolecular distances are observed around the *tert*-butyl groups of the BDA cations, which suggest the presence of hydrophobic van der Waals interactions as the main interaction (indicated by blue and white areas, Figure 5). In **2**, similar behaviour is observed, although a small number of closer intermolecular contacts with the anion oxo shell can be seen (indicated by red areas, Figure 5). For **3**, the *tert*-butyl groups show a larger number of close intermolecular contacts, which suggests that the number of hydrophobic, long-range interactions is more limited compared to the BDA cations in **1** and **2**. Based on these observations, the initial crystallographic study can be substantiated and further evidence is provided to suggest that a decreasing contribution of hydrophobic interaction modes is observed when comparing the BDA cations in **1**, **2** and **3**.

Conclusions

In conclusion, it has been shown that hybrid organic-inorganic frameworks can be assembled by the combination of amphiphilic BDA cations with a range of inorganic isopolyoxomolybdate cluster anions. To understand the complex modes of interaction between the organic BDA cations and the inorganic cluster building units, three new hybrid polyoxomolybdate-based networks were synthesized and structurally analyzed to detect the presence of hydrophobic areas within the crystal lattice. It was shown that hydrophobic packing effects are observed in **1** and **2**, in which the anion size is comparable to the size of the organic cation employed. For **3**, it was shown that when a very large cluster anion is used, the packing requirements of the cluster within the lattice are dominant and no pronounced hydrophobic aggregation was observed. These findings were substantiated by a theoretical Hirshfeld analysis of the BDA counterions that suggested that a higher number of close intermolecular distances is observed in **3**, which indicate a decrease in the number of long-range hydrophobic interactions of the *tert*-butyl substituent in the BDA cations. This clearly demonstrates the limitations of the synthetic route presented. In addition, it has to be noted that the crystal packing is controlled by a multitude of interactions that range from attractive and repulsive electrostatic interactions to hydrogen bonding and van der Waals interactions, and all attempts to design supramolecular crystal lattices need to take into account the complex combination of this range of interactions. Furthermore, it was shown that the inorganic counterion plays a crucial role as it is often incorporated as a sterically nondemanding, charge-balancing unit. In future studies larger amphiphilic counterions, such as cetyltrimethylammonium, will be employed in the $\{Mo_{36}\}$ system to understand whether structural control can be increased towards larger cluster systems. In addition, studies under sodium-free conditions will be used to evaluate the hydrophobic effects in purely BDA–molybdate systems.

Experimental Section

Materials and Methods: All chemicals were purchased from Sigma Aldrich and Acros (reagent grade) and were used as received. FTIR spectra (KBr pellets) were measured with a Shimadzu FT-IR-8400S FTIR spectrometer. Elemental analyses were carried out with a Euro Vector Euro EA 3000 elemental analyzer. Thermogravimetric analyses (TGA) were performed with a TA Q50 thermogravimetric analyzer. UV/Vis spectra were recorded with a Varian Cary 50 UV/Vis spectrophotometer or a Shimadzu PharmaSpec 1700 UV/Vis spectrophotometer. Powder XRD analysis was performed with a Philips X′PERT 1 powder diffractometer.

$Na_5[tBuNH(C_2H_4OH)_2][Mo_7O_{24}]\cdot ca.\ 14H_2O$ (1): To a solution of Na_2MoO_4 (3.00 g, 12.4 mmol) in deionized water (60 mL) was added $tBuN(C_2H_4OH)_2$ (10.0 g, 62.0 mmol, 5 equiv.), and the resulting solution was stirred vigorously for 30 min. The pH was adjusted to 5.5 by the dropwise addition of HCl (1 M). The light yellow, clear solution was stored in a beaker and slow evaporation over the course of two weeks gave colourless crystalline blocks of **1**. The crystals were washed with cold water and ethanol, collected by filtration and air-dried; yield 1.24 g (0.80 mmol; 51.6% based on Mo). IR: $\tilde{\nu}$ = 3500 (s, b), 3059 (m), 2980 (m), 2598 (w), 1630 (w), 1480 (m), 1456 (m), 1410 (m), 1383 (m), 1364 (m), 1302 (m), 1184 (m), 1084 (s), 1046 (m), 1003 (m), 950 (s), 920 (s), 850 (s), 720 (s), 654 (s) cm^{-1}. $C_8H_{20}Mo_7N_1Na_5O_{39.5}$ (1540.76): calcd. C 6.20, H 1.30, N 0.90; found C 6.32, H 1.45, N 0.97. TGA water loss from r.t. to 120° C (wt.-%): calcd. 16.1; found 13.2.

$[tBuNH(C_2H_4OH)_2]_4[Mo_8O_{26}]\cdot ca.\ 4H_2O$ (2): To a solution of Na_2MoO_4 (3.00 g, 12.4 mmol) in deionized water (60 mL) was added $tBuN(C_2H_4OH)_2$ (10.0 g, 62.0 mmol, 5 equiv.), and the solution was stirred vigorously for 30 min. The pH value was adjusted to 4.0 by the dropwise addition of aqueous HCl (1 M). The resulting solution was stored in a beaker and slow evaporation over the course of ten days gave colourless crystals of **2**. The crystals were washed with cold water and ethanol, collected by filtration and dried; yield 0.636 g (0.35 mmol, 45.6% based on Mo). IR: $\tilde{\nu}$ = 3414 (s, b), 3082 (m), 2984 (m), 2781 (w), 1478 (m), 1383 (m), 949 (s), 912 (s), 843 (s) cm^{-1}. $C_{32}H_{80}Mo_8N_4O_{38}$ (1896.51): calcd. C 20.97, H 4.40, N 3.06; found C 21.03, H 4.37, N 3.03. TGA water loss from r.t. to 120° C (wt.-%): calcd. 3.8; found 3.2.

$[tBuNH(C_2H_4OH)_2]_{14}[Mo_{36}O_{112}(H_2O)_{16}][Mo_{36}O_{112}(H_2O)_{14}\{tBuNH(C_2H_4OH)_2\}_2]\cdot ca.\ 36H_2O$ (3): To a solution of Na_2MoO_4 (1.00 g, 4.13 mmol) in deionized water (40 mL) was added $tBuN(C_2H_4OH)_2$ (0.668 g, 4.14 mmol, 1 equiv.), and the solution was stirred vigorously for 30 min. The pH was adjusted to 2.0 by the dropwise addition of aqueous HCl (1 M). The resulting, slightly yellow solution was kept in a beaker and slow evaporation over ca. three weeks gave colourless crystals of **3**. The crystals were washed with cold water and ethanol, collected and dried; yield 0.603 g (84.3 μmol, 73.4% based on Mo). IR: $\tilde{\nu}$ = 3451 (b), 2997 (m), 2795 (m), 1385 (m), 1184 (w), 1082 (m), 957 (s), 883 (s), 864 (s), 800 (s) cm^{-1}. $C_{128}H_{448}Mo_{72}N_{16}O_{320}$ (14237.59): calcd. C 10.80, H 3.17, N 1.57; found C 10.86, H 3.28, N 1.54. TGA water loss from r.t. to 120° C (wt.-%): calcd. 4.3; found 3.8.

Crystallographic Details: Suitable single crystals of **1**, **2** and **3** were mounted on to the end of a thin glass fibre using Fomblin oil. X-ray diffraction intensity data were measured at 150 K with a Nonius Kappa CCD diffractometer [λ(Mo-K_α) = 0.71073 Å] equipped with a graphite monochromator. Structure solution and refinement was carried out using the SHELX-97 package with WinGX. Corrections for incident and diffracted beam absorption effects were applied using empirical or numerical methods. Structures were solved by a combination of direct methods and difference Fourier syntheses and refined against F^2 by the full-matrix least-squares technique. Crystal data, data collection parameters and refinement statistics are listed in Table 1.

Table 1. Crystallographic data for **1**–**3**.

	1	**2**	**3**
Formula	$C_8H_{20}Mo_7N_1Na_5O_{39.5}$	$C_{32}H_{80}Mo_8N_4O_{38}$	$C_{128}H_{512}Mo_{72}N_{16}O_{318.8}$
M_r [g mol^{-1}]	1548.76	1896.50	14221.32
Crystal system	triclinic	triclinic	monoclinic
Space group	$P\bar{1}$	$P\bar{1}$	$P2_1/c$
a [Å]	11.1832(10)	11.1208(7)	25.745(5)
b [Å]	19.409(2)	12.4050(9)	26.688(5)
c [Å]	20.1284(11)	13.2032(6)	28.521(6)
α [°]	73.939(5)	63.451(4)	90
β [°]	86.312(7)	85.560(5)	96.55(3)
γ [°]	87.584(8)	68.902(6)	90
$\rho_{calcd.}$ [g cm^{-3}]	2.424	1.994	2.438
V [Å]	4188.4(6)	1512.52(16)	19468(7)
Z	4	1	2
μ [mm^{-1}]	2.194	1.698	2.344
T [K]	150(2)	150(2)	150(2)
F(000)	2880	860	12928
min., max. θ [°]	3.57, 26.37	2.75, 30.00	3.52, 26.37
Measured refl.	130361	51315	257157
Unique refl.	17052	8814	36876
Parameters	1090	444	2531
GooF	1.103	1.096	1.102
$R1$ [$I > 2\sigma(I)$]	0.0236	0.0263	0.0506
$wR2$ (all data)	0.0587	0.0927	0.1179

CCDC-807932 (for **1**), -807933 (for **2**) and -807934 (for **3**) contain the supplementary crystallographic data for this paper. These data can be obtained free of charge from The Cambridge Crystallographic Data Centre via www.ccdc.cam.ac.uk/data_request/cif.

Hirshfeld Surface Analysis: Hirshfeld analysis was carried out using CrystalExplorer (v2.1) by K. Wolff, D. J. Grimwood, J. J. McKinnon, M. J. Turner, D. Jayatilaka, M. A. Spackman, University of Western Australia, 2010. Hirshfeld surfaces were generated based on all molecular fragments within a radius of 5.0 Å around a given BDA molecule. The colour-coded isosurface visualization is based on normalized intermolecular distances d_{norm}, where $d_{norm} = [(d_i - r_{i,vdW})/r_{i,vdW}] + [(d_e - r_{e,vdW})/r_{e,vdW}]$ with $d_{i/e}$ = internal/external distance between the Hirshfeld surface and the nucleus; $r_{i/e,vdW}$ = van der Waals radius of the internal/external nucleus. For details see ref.[23]

Supporting Information (see footnote on the first page of this article): Detailed information of the syntheses, analyses and Hirshfeld analyses.

Acknowledgments

The authors gratefully acknowledge the support by the Institute of Inorganic Chemistry II (FAU). The Fonds der Chemischen Industrie (FCI) is gratefully acknowledged for providing a Liebig Fellowship (to C. S.) and a doctoral fellowship (to J. F.).

[1] a) V. Balzani, M. Gomez-Lopez, J. F. Stoddart, *Acc. Chem. Res.* **1998**, *31*, 405–414; b) N. R. Champness, *Angew. Chem.* **2009**, *121*, 2309; *Angew. Chem. Int. Ed.* **2009**, *48*, 2274–2275; c) J. F. Stoddart, *Chem. Soc. Rev.* **2009**, *38*, 1802–1820; d) D.

Braga, *J. Chem. Soc., Dalton Trans.* **2000**, 3705–3713; e) J. M. Lehn, *Science* **2002**, *295*, 2400–2403.

[2] a) G. M. Whitesides, J. P. Mathias, C. T. Seto, *Science* **1991**, *254*, 1312–1319; b) Z. R. Chen, J. A. Kornfield, S. D. Smith, J. T. Grothaus, M. M. Satkowski, *Science* **1997**, *277*, 1248–1253; c) S. Park, J. H. Lim, S. W. Chung, C. A. Mirkin, *Science* **2004**, *303*, 348–351; d) L. C. Palmer, Y. S. Velichko, M. O. de la Cruz, S. I. Stupp, *Phil. Trans. Roy. Soc. A* **2007**, *365*, 1417–1433; e) P. Besenius, G. Portale, P. H. H. Bomans, H. M. Janssen, A. R. A. Palmans, E. W. Meijer, *Proc. Natl. Acad. Sci. USA* **2010**, *107*, 17888–17893.

[3] a) R. Kawamoto, S. Uchida, N. Mizuno, *J. Am. Chem. Soc.* **2005**, *127*, 10560–10567; b) Y. S. Bae, O. K. Farha, A. M. Spokoyny, C. A. Mirkin, J. T. Hupp, R. Q. Snurr, *Chem. Commun.* **2008**, 4135–4137.

[4] a) M. Dinca, J. R. Long, *Angew. Chem.* **2008**, *120*, 6870; *Angew. Chem. Int. Ed.* **2008**, *47*, 6766–6779; b) X. Lin, J. H. Jia, X. B. Zhao, K. M. Thomas, A. J. Blake, G. S. Walker, N. R. Champness, P. Hubberstey, M. Schröder, *Angew. Chem.* **2006**, *118*, 7518; *Angew. Chem. Int. Ed.* **2006**, *45*, 7358–7364; c) N. L. Rosi, J. Eckert, M. Eddaoudi, D. T. Vodak, J. Kim, M. O'Keeffe, O. M. Yaghi, *Science* **2003**, *300*, 1127–1129.

[5] a) J. Ruokolainen, G. ten Brinke, O. Ikkala, *Adv. Mater.* **1999**, *11*, 777–780; b) C. P. Pradeep, D. L. Long, G. N. Newton, Y. F. Song, L. Cronin, *Angew. Chem.* **2008**, *120*, 4460; *Angew. Chem. Int. Ed.* **2008**, *47*, 4388–4391; c) J. A. A. W. Elemans, A. E. Rowan, R. J. M. Nolte, *J. Mater. Chem.* **2003**, *13*, 2661–2670.

[6] T. F. Fässler, R. Hoffmann, *Angew. Chem.* **1999**, *111*, 526; *Angew. Chem. Int. Ed.* **1999**, *38*, 543–546.

[7] a) P. D. Godfrey, W. J. Grigsby, P. J. Nichols, C. L. Raston, *J. Am. Chem. Soc.* **1997**, *119*, 9283–9284; b) M. J. Hardie, C. L. Raston, *Chem. Commun.* **2001**, 905–906.

[8] a) M. Schulz-Dobrick, M. Jansen, *CrystEngComm* **2008**, *10*, 661–664; b) M. Schulz-Dobrick, M. Jansen, *Angew. Chem.* **2008**, *120*, 2288; *Angew. Chem. Int. Ed.* **2008**, *47*, 2256–2259.

[9] K. K. Rangan, P. N. Trikalitis, M. G. Kanatzidis, *J. Am. Chem. Soc.* **2000**, *122*, 10230–10231.

[10] M. T. Pope, A. Müller, *Polyoxometalate Chemistry: from Topology via Self-Assembly to Applications*, Springer Verlag, New York, **2001**.

[11] P. Judeinstein, C. Sanchez, *J. Mater. Chem.* **1996**, *6*, 511–525.

[12] C. Streb, L. Long, L. Cronin, *Chem. Commun.* **2007**, 471–473.

[13] a) C. Streb, D. L. Long, L. Cronin, *CrystEngComm* **2006**, *8*, 629–634; b) C. Streb, T. McGlone, O. Brücher, D. L. Long, L. Cronin, *Chem. Eur. J.* **2008**, *14*, 8861–8868.

[14] a) C. J. Jiang, A. Lesbani, R. Kawamoto, S. Uchida, N. Mizuno, *J. Am. Chem. Soc.* **2006**, *128*, 14240–14241; b) Y. Ishii, Y. Takenaka, K. Konishi, *Angew. Chem.* **2004**, *116*, 2756; *Angew. Chem. Int. Ed.* **2004**, *43*, 2702–2705; c) J. Forster, B. Rösner, M. M. Khusniyarov, C. Streb, *Chem. Commun.* **2011**, *47*, 3114–3116.

[15] a) M. T. Pope, *Heteropoly and Isopoly Oxometalates*, Springer-Verlag, Heidelberg, Germany, **1983**; b) H. Abbas, C. Streb, A. L. Pickering, A. R. Neil, D. L. Long, L. Cronin, *Cryst. Growth Des.* **2008**, *8*, 635–642; c) Y. Lu, Y. Xu, E. B. Wang, J. Lu, C. W. Hu, L. Xu, *Cryst. Growth Des.* **2005**, *5*, 257–260; d) X. Y. Wu, C. Z. Lu, Q. Z. Zhang, S. M. Chen, X. J. Xu, *J. Coord. Chem.* **2006**, *59*, 2047–2054.

[16] a) J. J. Hastings, O. W. Howarth, *J. Chem. Soc., Dalton Trans.* **1992**, 209–215; b) R. I. Maksimovskaya, G. M. Maksimov, *Inorg. Chem.* **2007**, *46*, 3688–3695; c) L. Pettersson, *Mol. Eng.* **1993**, *3*, 29–42.

[17] M. Grabau, J. Forster, K. Heussner, C. Streb, *Eur. J. Inorg. Chem.* **2011**, 1719–1724.

[18] a) L. R. Pratt, D. Chandler, *J. Chem. Phys.* **1977**, *67*, 3683–3704; b) B. Widom, K. Koga, P. Bhimalapuram, *Mol. Phys.* **2002**, *100*, 3795–3801; c) B. Widom, P. Bhimalapuram, K. Koga, *Phys. Chem. Chem. Phys.* **2003**, *5*, 3085–3093.

[19] a) T. Arumuganathan, A. S. Rao, S. K. Das, *Cryst. Growth Des.* **2010**, *10*, 4272–4284; b) V. Coue, R. Dessapt, M. Bujoli-Doeuff, M. Evain, S. Jobic, *Inorg. Chem.* **2007**, *46*, 2824–2835; c) P. Roman, A. Luque, A. Aranzabe, J. M. Gutierrez-Zorrilla, *Polyhedron* **1992**, *11*, 2027–2038.

[20] I. D. Brown, *J. Appl. Crystallogr.* **1996**, *29*, 479–480.

[21] a) H. Jin, Y. F. Qi, E. B. Wang, Y. G. Li, X. L. Wang, C. Qin, S. Chang, *Cryst. Growth Des.* **2006**, *6*, 2693–2698; b) C. J. Zhang, H. J. Pang, Q. Tang, H. Y. Wang, Y. G. Chen, *Dalton Trans.* **2010**, *39*, 7993–7999; Y. Q. Lan, S. L. Li, X. L. Wang, K. Z. Shao, Z. M. Su, E. B. Wang, *Inorg. Chem.* **2008**, *47*, 529–534.

[22] a) B. Krebs, I. Paulat-Böschen, *Acta Crystallogr., Sect. B* **1982**, *38*, 1710–1718; b) R. Atencio, A. Briceno, X. Galindo, *Chem. Commun.* **2005**, 637–639; c) K. Eda, Y. Iriki, *Chem. Lett.* **2005**, *34*, 612–613; d) D. L. Long, C. Streb, P. Kögerler, L. Cronin, *J. Cluster Sci.* **2006**, *17*, 257–266.

[23] a) M. A. Spackman, J. J. McKinnon, *CrystEngComm* **2002**, 378–392; b) M. A. Spackman, D. Jayatilaka, *CrystEngComm* **2009**, *11*, 19–32; c) J. J. McKinnon, M. A. Spackman, A. S. Mitchell, *Acta Crystallogr., Sect. B* **2004**, *60*, 627–668; d) J. J. McKinnon, D. Jayatilaka, M. A. Spackman, *Chem. Commun.* **2007**, 3814–3816.

[24] a) C. Roetti, E. Clementi, *J. Chem. Phys.* **1974**, *60*, 3342–3342; b) C. Roetti, E. Clementi, *J. Chem. Phys.* **1974**, *60*, 4725–4729; c) E. Clementi, C. Roetti, *At. Data Nucl. Data Tables* **1974**, *14*, 177–478.

Received: July 2, 2011
Published Online: October 21, 2011

